Sains Malaysiana 51(10)(2022): 3251-3259
http://doi.org/10.17576/jsm-2022-5110-11

Hydrogen Production from Water Splitting using TiO_2/CoS Composite Photocatalyst

(Penghasilan Hidrogen daripada Pemisahan Air menggunakan Komposit Fotomangkin TiO_2/CoS)

MUTIA AGUSTINA[1], SITI NURUL FALAEIN MORIDON[2], AMILIA LINGGAWATI[1], KHUZAIMAH ARIFIN[2,*], LORNA JEFFERY MINGGU[2] & MOHAMMAD B. KASSIM[3]

[1]*Department of Chemistry, Faculty of Mathematic and Natural Science, University of Riau, Kampus Binawidya, Km 12.5, Simpang Baru, Pekanbaru Riau, Indonesia*
[2]*Fuel Cell Institute, Universiti Kebangsaan Malaysia, 43600 UKM Bangi, Selangor Darul Ehsan, Malaysia*
[3]*Department of Chemical Sciences, Faculty of Science and Technology, Universiti Kebangsaan Malaysia, 43600 UKM Bangi, Selangor Darul Ehsan, Malaysia*

Received: 8 February 2022/Accepted: 1 June 2022

ABSTRACT

Photocatalytic water splitting reaction has been considered an ideal method for hydrogen generation. In this study, a composite of TiO_2/CoS photocatalyst prepared by hydrothermal synthesis method assisted by ball milling crushing process was used. The TiO_2/CoS composites prepared with three variation compositions of 90/10, 80/20, and 70/30 were named M-10, M-20, and M-30, respectively. Field-emission scanning electron microscopy images showed that the morphologies of the composites were porous and uniform of nanospheres. The X-ray diffraction and energy dispersive spectroscopy analyses confirmed the presence of CoS in the composites. Ultraviolet–visible absorption characterization demonstrated the smallest bandgap value of approximately 2.72 eV presented by sample M-30 with the photocurrent density of 0.32 mA cm^{-2} at 0.9 V vs. Ag/AgCl. The presence of CoS in this study could increase the PC hydrogen generation of TiO_2 by nearly 2.5 times. The composites forming a p-n heterojunction between TiO_2 and CoS could prevent electron–hole recombination and increase the overall photoactivity of TiO_2.

Keywords: Composite; hydrogen production; hydrothermal; water splitting

ABSTRAK

Tindak balas pemisahan air secara fotokatalisis telah dianggap sebagai kaedah yang ideal untuk penjanaan hidrogen dengan menggunakan semikonduktor sebagai fotomangkin. Dalam kajian ini, komposit fotomangkin TiO_2/CoS yang disediakan melalui kaedah sintesis hidroterma dibantu oleh proses penghancuran penggilingan bebola telah digunakan. Komposit TiO_2/CoS yang disediakan dengan tiga komposisi variasi 90/10, 80/20 dan 70/30 masing-masing dinamakan M-10, M-20 dan M-30. Imej mikroskopi elektron pengimbasan pelepasan medan menunjukkan bahawa morfologi komposit adalah berliang dan nanosfera yang seragam. Analisis difraksi sinar-X dan spektroskopi penyebaran tenaga mengesahkan kehadiran CoS dalam komposit. Pencirian penyerapan cahaya ultraungu-nampak menunjukkan nilai celah jalur terkecil kira-kira 2.72 eV yang ditunjukkan oleh sampel M-30 dengan ketumpatan arus foto 0.32 mA cm^{-2} pada 0.9 V lwn. Ag/AgCl. Kehadiran CoS dalam kajian ini boleh meningkatkan penjanaan hidrogen PC TiO_2 sebanyak hampir 2.5 kali ganda. Komposit yang membentuk hetero-simpang p-n antara TiO_2 dan CoS boleh mengurangkan penggabungan semula lohong serta elektron dan meningkatkan keseluruhan fotoaktiviti TiO_2.

Kata kunci: Hidroterma; komposit; pemisahan air; pengeluaran hidrogen

INTRODUCTION

Hydrogen has been considered a future clean and environmentally friendly energy carrier to replace fossil fuel. Hydrogen is used in fuel cell systems to generate electricity with only pure water as byproduct (Rosen & Koohi-Fayegh 2016). However, hydrogen gas is not found naturally as a gas on earth; specifically, it needs to be extracted from various sources, such as hydrocarbon, water, acid, or other molecules (Scott 2019). Nearly 95% of hydrogen is currently produced from hydrocarbon fossil fuels by means of gas reforming and gasification coal processes, which have limited resources and not clean processes. Meanwhile, hydrogen from abundant water resources is only around 4% (Franchi et al. 2020). The water splitting process used to generate hydrogen gas requires high energy of approximately 237.2 KJ/mol. The most potential method to produce hydrogen from water is to use direct solar light energy imitating natural photosynthesis. Such hydrogen production method has cost and space saving compared with conventional solar hydrogen method that uses photovoltaic and electrolyzer (Guo et al. 2015).

Direct water splitting has two methods: photocatalytic (PC) and photoelectrochemical (PEC). The PC method uses photocatalyst in suspension form or in homogenous catalysis system, while PEC method uses separated photoelectrode anode and cathode or in heterogenous catalysis system. The active material of photocatalyst or photoelectrode should be a semiconductor, and titanium dioxide (TiO_2) is among widely investigated semiconductors (Moridon et al. 2021). TiO_2 has several advantages, such as photoactive nature, good photo and chemical stability, abundance, low cost, and nontoxicity (Arifin et al. 2021; Dincer et al. 2015; Liu et al. 2016). However, TiO_2 has around 3.2 eV bandgap that limits the solar energy that could be utilized to only ultraviolet (UV) energy, which accounts for 4% of the solar spectrum. Meanwhile, most solar energy considered to be visible (vis) light energy cannot be used. The wide bandgap also causes the separated photogenerated electron and hole to easily recombine.

Few methods are used to overcome the wide bandgap problem of TiO_2, and one of them is to produce a composite heterojunction with semiconductor materials. Several composite heterojunctions have shown to produce significant results, for example, Liu et al. (2018) used a TiO_2/CdS nanostructure that produced a much more remarkable photocurrent density of 9.65 mA/cm^2 at 0.80 V vs RHE, much higher than pristine TiO_2 photocurrent density. The heterojunction is forming Z scheme band structure that could reduce charge recombination. Considering CdS is a highly toxic material, other metal chalcogenides as the co-catalysts to TiO_2 have been widely investigated. Here, we investigated the composite of TiO_2 with CoS and explored the produced photocurrent and the generated hydrogen. CoS is widely used in photoelectrochemistry because of its good electrochemical activity, nontoxicity, and relatively low cost (Liu et al. 2018; Moridon et al. 2019; Niu et al. 2018). CoS is a p-type semiconductor with a bandgap of approximately 2.6 eV, and with TiO_2 is supposed to produce a type-2 heterojunction, similar to CdS (Ouyong et al. 2018). Niu et al. (2018) has reported CoS as a co-catalyst of TiO_2 for PEC water splitting, in which the hydrogen generated by 20% CoS/TiO_2 composite in aqueous methanol solution is ~18-fold higher than pure TiO_2. However, the impact of CoS composition in the composite has not been reported yet. In this study, the composition of TiO_2 and CoS in the composite will be evaluated. The composites synthesized by hydrothermal method assisted by ball milling process to crush the bulk powder into a nanosize material. The composite performance evaluated by measuring the photocurrent density and the produced hydrogen gas.

MATERIALS AND METHODS

CHEMICALS

The chemicals used were TiO_2 P25 (Degussa AG D-60297 Frankfurt), ethanol (R&M Chemicals), acetone (R&M Chemicals), cobalt nitrate hexahydrate ($Co(NO_3)_2.6H_2O$; Sigma–Aldrich), thiourea (MERCK), nitrogen (Linde), fluorine-doped tin oxide (FTO) glass, and polyethylene glycol (PEG; R&M Chemicals).

SYNTHESIS OF TiO_2/CoS COMPOSITES

In this work, 1.46 g of $Co(NO_3)_2.6H_2O$ and 0.38 g of thiourea were dissolved in a solution of 20 mL of ethanol and 5 mL of distilled water (Rambey et al. 2020). The solution was sonicated for 30 min and then poured into a Teflon lined with stainless steel autoclave. Thereafter, the autoclave was heated at 180 °C for 24 h in the oven, and the resulting precipitation was filtered and washed alternately using distilled water and ethanol. The precipitation product CoS was dried at 60 °C for 12 h and calcined at 400 °C for 12 h.

The TiO_2/CoS composites were prepared following the method used by Wang et al. (2013) in three variations of weight ratios (10%, 20%, and 30%) of CoS and TiO_2. Each sample variation was dissolved into 70 mL of acetone and then stirred for 30 min. The stirring was continued with heating at 40 °C until the entire solvent had evaporated such that TiO_2/CoS solids could be obtained. The 1 g of TiO_2/CoS powder mixed with 0.25 g of PEG and 8 mL of ethanol was poured into a ceria container with the balls, and the milling process was conducted at 3000 rpm for 2 h. The ball milling process ensures homogeneity of particles in the mixture and high density among particles. The formed slurry was casted on the cleaned FTO glass and then annealed at 400 °C for 2 h. Samples were labeled as ‘M-10’, ‘M-20’, and

'M-30' for TiO_2/CoS with weight ratios of 90:10, 90:20, and 90:30, respectively.

STRUCTURAL CHARACTERIZATIONS

The morphology of the composite was characterized by field-emission scanning microscopy (FESEM, ZEISS SUPRA 55VP). The X-ray diffraction (XRD) patterns were obtained using a diffractometer (Bruker D8-Advanced) with Cu Kα radiation (λ = 1.5418 Å). Meanwhile, UV–vis diffuse reflectance spectroscopy of the samples was collected using a UV/VIS/NIR spectrometer (Perkin Elmer Lambda 950) with a wavelength range of 200-850 nm.

MEASUREMENT OF PEC AND HYDROGEN PRODUCTION

PEC response was measured using Ametek VersaSTAT 4 under 100 $mWcm^{-2}$ Xenon light connected to a computer with the Versa Studio software. The instrument was operated using three electrodes: the sample as the working electrode, the Ag/AgCl electrode as the reference electrode, and the Pt wire as counter electrode. Meanwhile, Na_2SO_4 0,5 M (pH 7) used as the electrolyte solution. Linear scan voltammetry (LSV) was conducted with a scan rate of 0.01 V/s. The electrochemical impedance spectroscopy (EIS) was performed in dark condition at -0.5 V potential in the frequency range of 10000-0.1 Hz.

Hydrogen production measurement was performed using a 250 mL circular aluminum reactor with polytetrafluoroethylene (Teflon®) lining and a top quartz window. A 500-watt xenon lamp with an AM 1.5 was used as light source. A hydrogen sensor (UNISENSE) was used to measure the amount of produced hydrogen. The 0.25 g of samples dissolved in 50 mL of 0.5 M Na_2SO_4 solution (pH 7) was placed in the reactor and underwent degassing using N_2 gas. The suspension samples were placed under a light source for 1 h, and the obtained hydrogen was measured at 10 min intervals.

RESULTS AND DISCUSSION

CHARACTERIZATION OF STRUCTURE AND MORPHOLOGY

The grayish-white powder of the TiO_2/CoS composite was produced in two major steps as mentioned previously, and each sample was named according to its TiO_2/CoS weight ratio (i.e., M-10, M-20, and M-30). The FESEM characterization was conducted on TiO_2/CoS surface thin film with a magnification of 50,000 and 100,000 times (Figure 1(a) and 1(b)). The results show that the

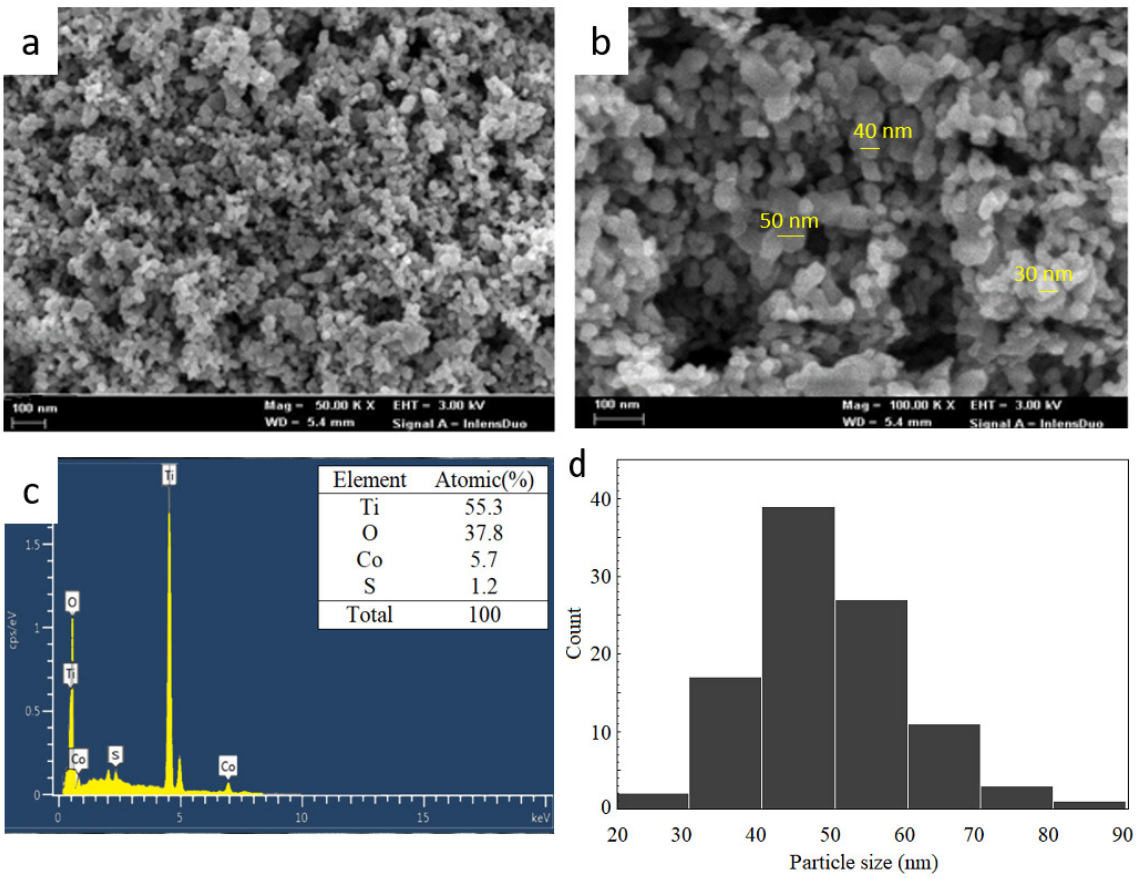

FIGURE 1. FESEM images of TiO_2/CoS composite (M-10) (a) with magnification 50.000×, (b) 100.000×, (c) EDS analysis, and (d) particle size distribution

composite is porous and has uniform particle shape of nanospheres. The 100 particle counts from FESEM images were analyzed, in which the nanosphere size ranged produced from 25.09 - 87.52 nm (Figure 1(c)). The most size is 40-50 nm and 50-60 nm, about 39% and 27%, respectively. Meanwhile, only about 2% in size of 20-30 nm and 80-90 nm. FESEM-EDS of sample M-10 shows the peaks of titanium (55.3%), oxygen (37.8%), cobalt (5.7%), and sulfur (1.2%). The presence of Co and S elements in the EDS characterization confirms the CoS in sample (Figure 1(d)) and supported by XRD analysis. Figure 2 shows the XRD diffractograms of TiO_2, CoS, and M-10 samples. Peaks appear at 33.50° (d_{100}) and 54.32° (d_{110}) in M-10 indicates the presence of CoS in the sample (Niu et al. 2018). Furthermore, peaks at 25.28° (d_{101}), 37.82° (d_{004}), 38,60° (d_{112}), 48.08°(d_{200}), 53.93° (d_{105}), and 55.12° (d_{211}) are for TiO_2 anatase; meanwhile, peaks at 27.44° (d_{110}), 36.17° (d_{101}), and 41.34° (d_{111}) are for rutile (JCPDS No. 21-1276). The peak with the highest intensity at 25.28° indicates that anatase is the dominant phase in the composites. In this study, we only used sample M-10, which has the lowest content of CoS among samples, in structure and morphology characterization. If CoS could be detected in sample M-10, the CoS should be present in samples M-20 and M-30.

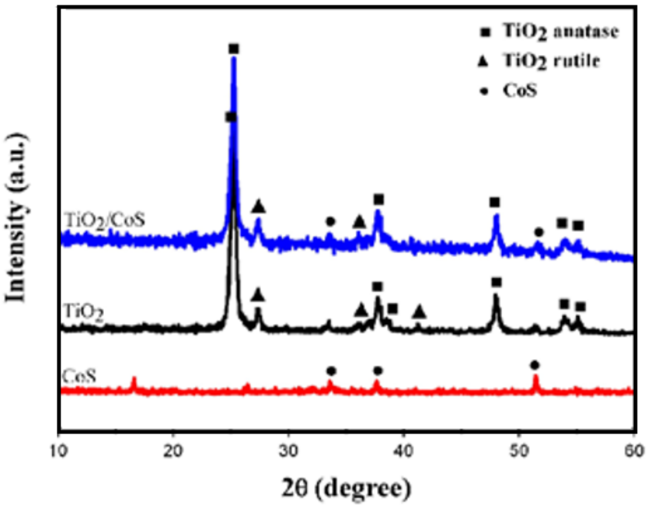

FIGURE 2. XRD diffractogram of CoS, TiO_2, and M-10

OPTICAL PROPERTIES

The optical properties of the composites in this study were determined by UV–vis absorption and EIS measurements. The UV–vis absorption of the pure TiO_2 and TiO_2/CoS composites is shown in Figure 3(a), where the pure TiO_2 absorbs light energy with the lowest molar absorption coefficients, while the highest is absorbed by sample M-30. In this study, the absorption ability of samples increases linearly with the increase in CoS content. The estimation bandgap value was determined from the absorption spectra using Tauc method based on the assumption that the energy-dependent absorption coefficient a can be expressed as

$$(\alpha . h\upsilon)^{1/\gamma} = B(h\upsilon - E_g) \tag{1}$$

where h is Planck's constant; υ is the frequency of the light; and γ factor depends on the nature of the electron transition and is equal to 1/2 or 2 for the direct or indirect transition band gap. Meanwhile, Eg is the band gap energy, and B is a constant (Makula 2018). The Tauc plot in Figure 3(b) shows that the pure TiO_2 produces a direct bandgap of approximately 3.3 eV. The bandgap value is reduced by the addition of CoS, where the direct bandgaps of M-10, M-20, and M-30 are 3.26, 2.83, and 2.72 eV, respectively. The bandgap energy obtained in this study is larger than the bandgap of TiO_2/CoS composite as reported by Niu et al. (2018) (nearly 2.1 eV). The different values might be because the number of CoS present in both studies was different because of differently the preparation method.

Besides the absorption and bandgap calculation, the PC water splitting activity is also determined by its charge density (N_A), valence band (V_B), and conduction band (C_B) positions. Combination of absorption and EIS data is used to estimate all the information. The charge transfer resistance (Rct) through Nyquist plot from the EIS results is shown in Figure 3(c). As observed, M-30 has the smallest semicircle, which means it has the largest resistance among the samples. By contrast, the pure TiO_2 has the lowest resistance. The Rct results agree with the bandgap calculation results. The N_A and flat-band potential (V_{FB}) values of the sample were determined through the Mott–Schottky plots (Figure 3(d)) derived from the equation below:

$$\frac{1}{C^2} = \left(\frac{2}{e\varepsilon\varepsilon_0 N_A}\right)\left[V - V_{FB} - \frac{K_b T}{e}\right], \tag{2}$$

where the slope of the plot between the reciprocal of the square $1/C^2$ and the bias potential are calculated as the carrier density N_A. Meanwhile, the x-intercept value is the V_{FB} (Figure 3(d)). The V_B and C_B positions can be determined using Equation (3) (Hankin et al. 2019):

$$E_{FB} - E_{VB} = k_B T ln \frac{N_V}{N_A} \tag{3}$$

Figure 3(d) shows that the highest N_A of 2.264 × 10^{10} cm^{-3} is produced by M-30, followed by M-20, M-10, and pure TiO_2 (Table 1). The flat-band potentials V_{FB} shift to a more positive potential with the increase in CoS content. The combination of V_{FB}, valence band (V_B), and conduction band (C_B) describes the ability in the PC water splitting process (Figure 4), where the band edge positions, and the bandgap of the composite become more appropriate for PC water splitting of hydrogen generation than related TiO_2.

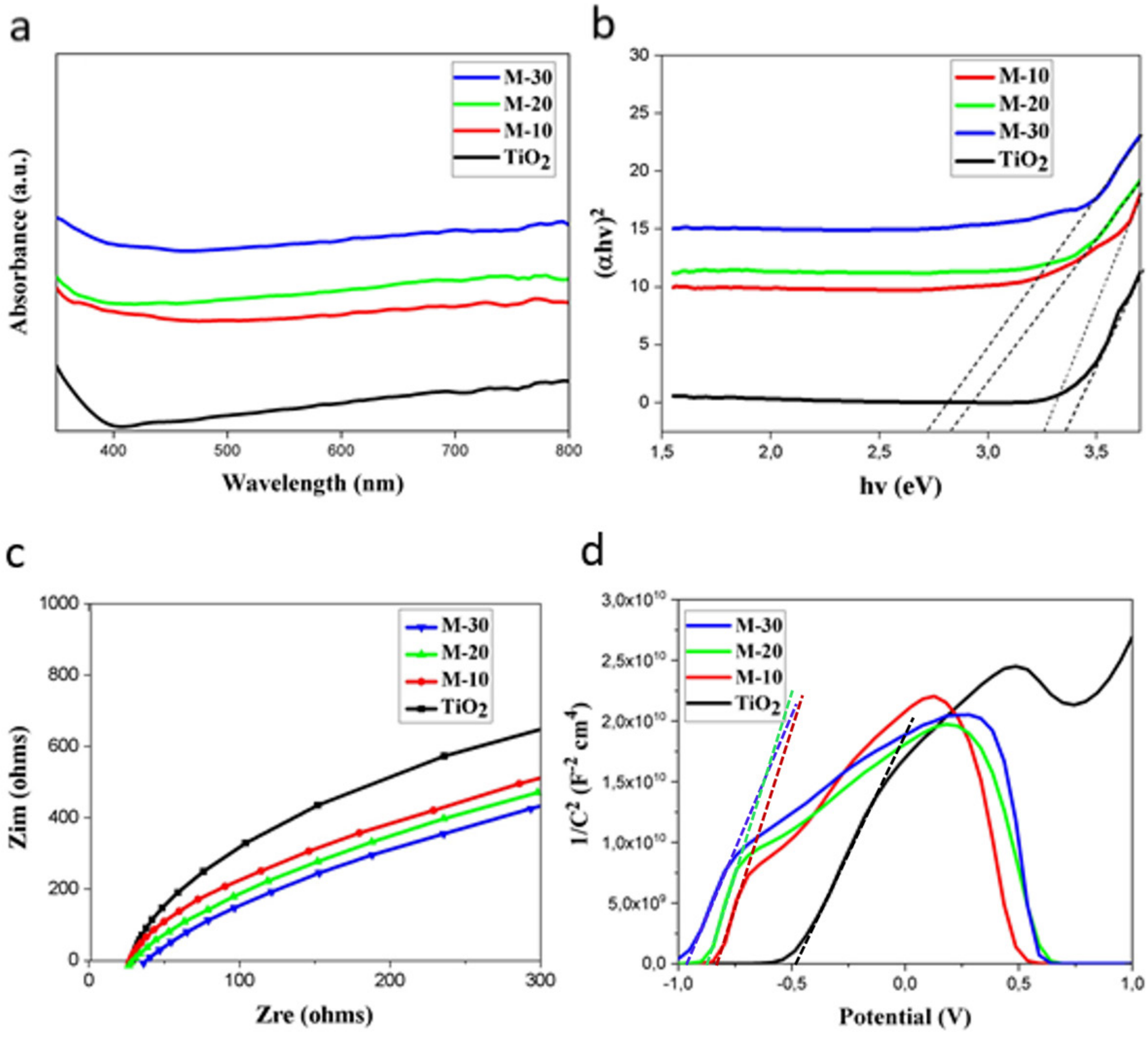

FIGURE 3. (a) Absorbance spectrum, (b) bandgap energy, and (c) Nyquist plots, and (d) Mott–Schottky plots of pure TiO_2, M-10, M-20, and M-30

TABLE 1. Electronic properties of TiO_2, M-10, M-20 and M-30

Photocatalyst	N_A (cm^{-3})	V_{fb}	V_B
TiO_2	1.829×10^{10}	-0.48	2.62
M-10	1.736×10^{10}	-0.79	2.27
M-20	1.835×10^{10}	-0.86	1.77
M-30	2.264×10^{10}	-0.95	1.57

MEASUREMENT OF PEC PERFORMANCE AND HYDROGEN PRODUCTION

The photocurrent density values were determined using LSV measurement from the difference current densities under dark and light conditions, as shown in Figure 5(a). All the composite samples produce higher photocurrent density than pure TiO_2. Sample M-30 produces the highest photocurrent density of around 0.32 mA cm^{-2} at 0.9 V vs. Ag/AgCl. The value is nearly 10-fold higher than that of the pure TiO_2 photocurrent density of around 35 μA cm^{-2} at 1 V. Meanwhile, M-10 and M-20 produce 0.16 and 0.18 mA cm^{-2} at 0.4 and 0. 0.65 V, respectively. In this study, the presence of CoS not only increases the photocurrent density but also shifts the onset potential to lower energy. The magnitude of the photocurrent density of the composite indicates the number of generated electrons that will be involved in the H_2 production reaction (Dincer & Bicer 2018).

The produced hydrogen was measured using a hydrogen sensor under vis light without adding some sacrificial electron donor or external bias. The amount of hydrogen produced was measured every 10 min for 60 min. The use of reliable and sensitive hydrogen sensor is helpful to detect small amount of hydrogen generation (Herkert et al. 2020). The amount and rates of hydrogen production are shown in Figure 4(b)-4(c). The detected hydrogen concentration in the reactor atmosphere slowly increases during the reaction times until 30 min reaction process. Thereafter, the concentration of the hydrogen decreases. The decrease in produced hydrogen might be caused by saturation of reactants at the active site of photocatalyst (Molinari et al. 2019). The highest hydrogen production rate of 0.41 mmol $h^{-1}g^{-1}$ is obtained using M-30, about 2.5 times higher than the highest hydrogen produced by pure TiO_2 is 0.154 mmol L^{-1} after 30 min PC reaction. Meanwhile, the highest hydrogen amounts generated by M-10 and M-20 are 0.167 mmol L^{-1} (20 min) and 0.186 mmol L^{-1} (30 min), respectively. This study shows that the CoS significantly affects the PC activity of pure TiO_2, in which the results of hydrogen produced by the composites are greater than those by the pure TiO_2. The improvement in photocurrent density and hydrogen generation is described by the mechanism in Figure 4(d), where the composites form a type-2 heterojunction structure. In this structure, the V_B and C_B of CoS lie at a more positive potential than V_B and C_B of TiO_2. With this band structure position, some excited electrons from TiO_2 that cannot achieve their C_B can move to CoS hole. Therefore, the hole of TiO_2 will oxidize water molecules more efficiently. The CoS is a p-type semiconductor with the leaving charge as the electron, and it becomes the place for hydrogen ion to be reduced. Meanwhile, the hole of moving carriers will be moved to the hole of TiO_2. Moreover, the n-type semiconductor TiO_2 becomes a place where water oxidation will occur. Thus, this type of composite can produce hydrogen higher than that of pure TiO_2. However, compared with a similar study previously reported, the hydrogen generated in this study is relatively low. Niu et al. (2018) measured that the hydrogen produced by 20%-CoS/TiO_2 composite is approximately 5.6 mmol $h^{-1}g^{-1}$, which is 67 times higher than that of pure TiO_2. However, they added methanol (76%) as a sacrificial electron donor to the reaction. By contrast, the hydrogen measured in the current study only used 0.5 M of the Na_2SO_4 solution without adding a material as a source of hydrogen. The hydrogen in this study was produced purely from the water splitting molecule and not from the electrolyte or other source.

The hydrogen production of TiO_2/CoS composite in this research could still be improved by using higher CoS contain composition and other nanostructures of TiO_2 such as nanorods or nanotube 1D structures. More advanced preparation method of composites could also be used.

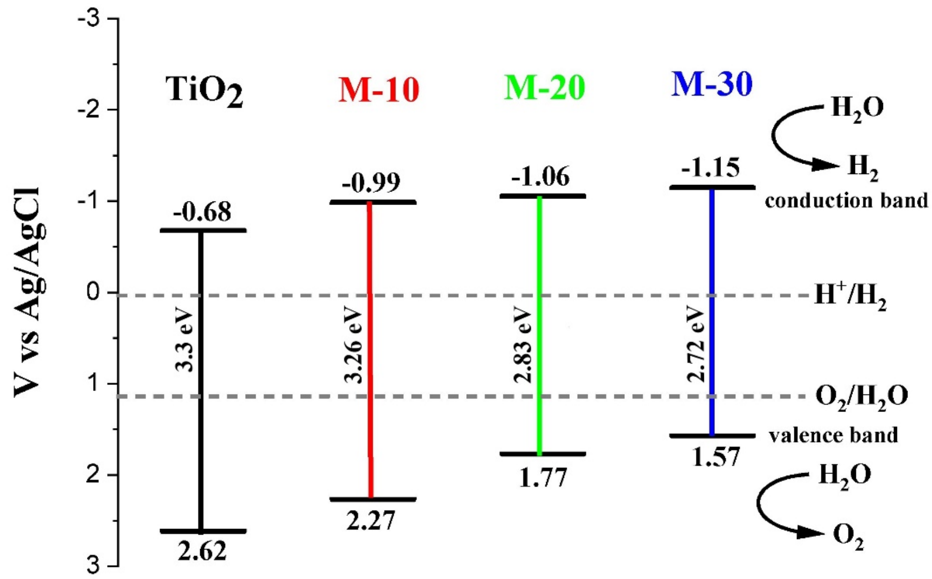

FIGURE 4. Band edge positions of pure TiO_2, M-10, M-20, and M-30 against redox potential water splitting using Ag/AgCl

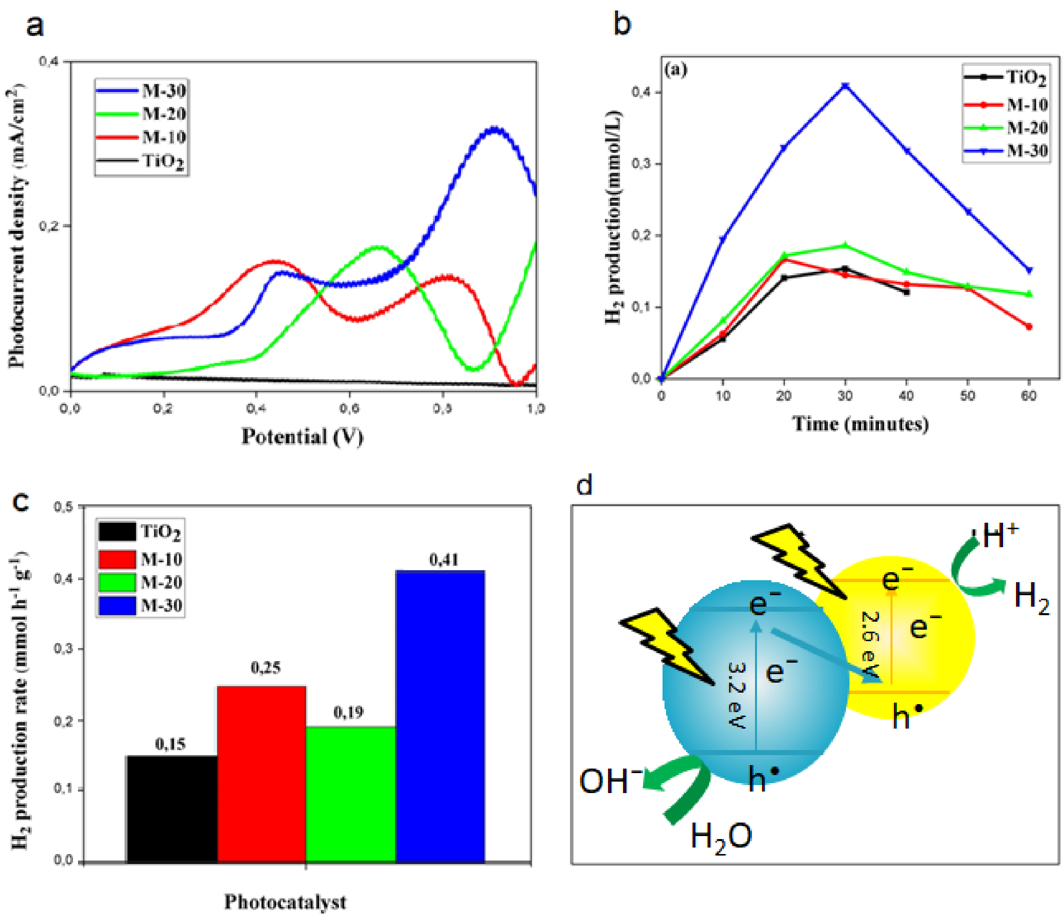

FIGURE 5. (a) Photocurrent density of pure TiO_2, M-10, M-20, and M-30; (b) hydrogen production and (c) hydrogen production rate of TiO_2, M-10, M-20, and M-30; and (d) mechanism of water oxidation and reduction on the TiO_2/CoS composite

Conclusion

The TiO_2/CoS composites were successfully synthesized and characterized under three varying percentages. The FESEM-EDS and XRD analyses confirmed the presence of CoS in the composites. The absorption and bandgap calculation results showed that the presence of CoS influenced the bandgap, as well as increased the photocurrent density measurement and hydrogen production. The highest photocurrent was produced by M-30, in which the value was approximately 10-fold of that produced by pure TiO_2 without CoS. Meanwhile, the rate of hydrogen production was nearly 2.5 times higher than that of the TiO_2. These overall results indicate that the presence of CoS could improve the PC ability of TiO_2. However, the results in this study still do not show the best composition, as the M-30 performance trend is still increasing. It is possible that by adding CoS content to the composite, the performance will be better than that of M-30.

Acknowledgements

This work was supported by the Ministry of Education, Malaysia under Research Grant FRGS/1/2019/STG01/UKM/03/2 and the Universiti Kebangsaan Malaysia under Publication Acceleration Fund PP-SELFUEL-2020.

References

Arifin, K., Yunus, R.M., Minggu, L.J. & Kassim, M.B. 2021. Improvement of TiO_2 nanotubes for photoelectrochemical water splitting: Review. *International Journal Hydrogen Energy* 46(7): 4998-5024. https://doi.org/10.1016/j.ijhydene.2020.11.063.

Dincer, I. & Acar, C. 2015. Review and evaluation of hydrogen production methods for better sustainability, I. *International Journal Hydrogen Energy* 40: 11094-11111. https://doi.org/10.1016/j.ijhydene.2014.12.035

Dincer, I. & Bicer, Y. 2018. Photoelectrochemical energy conversion. In *Comprehensive Energy Systems, Vol. 1. Energy Fundamental,* edited by Ibrahim Dincer. pp. 816-855. https://doi.org/10.1016/B978-0-12-809597-3.00438-7.

Franchi, G., Capocelli, M., De Falco, M., Piemonte, V. & Barba, D. 2020. Hydrogen production via steam reforming: A critical analysis of MR and RMM technologies. *Membranes* 10: 10. https://doi.org/10.3390/membranes10010010.

Guo, W., Zhang, X., Yu, R., Que, M., Zhang, Z., Wang, Z., Hua, Q., Wang, C., Wang, Z.L. & Pan, C. 2015. CoS NWs/Au hybridized networks as efficient counter electrodes for flexible sensitized solar cells. *Advanced Energy Materials* 5: 1500141. https://doi.org/10.1002/aenm.201500141.

Hankin, A., Bedoya-Lora, F.E., Alexander, J.C., Regoutz, A. & Kelsall, G.H. 2019. Flat band potential determination: Avoiding the pitfalls. *Journal of Materials Chemistry A* 7: 26162-26176. https://doi.org/10.1039/C9TA09569A.

Herkert, E., Sterl, F., Strohfeldt, N., Walter, R. & Giessen, H. 2020. Low-cost hydrogen sensor in the PPM range with purely optical readout. *ACS Sensors* 5(4): 978-983. https://doi.org/10.1021/acssensors.9b02314.

Liu, Y., Wang, Z. & Huang, W. 2016. Influences of TiO_2 phase structures on the structures and photocatalytic hydrogen production of CuO_x/TiO_2 photocatalysts. *Applied Surface Science* 389: 760-767. https://doi.org/10.1016/j.apsusc.2016.07.173.

Liu, C., Yang, Y., Lie, J. & Chen, S. 2018. Phase transformation synthesis of TiO_2/CdS heterojunction film with high visible-light photoelectrochemical activity. *Nanotechnology* 29: 265401. https://doi.org/10.1088/1361-6528/aabd6e

Makuła, P., Pacia, M. & Macyk, W. 2018. How to correctly determine the band gap energy of modified semiconductor photocatalysts based on UV–Vis spectra. *The Journal of Physical Chemistry Letters* 9(23): 6814-6817. https://doi.org/10.1021/acs.jpclett.8b02892.

Molinari, R., Lavorato, C., Argurio, P., Szymański, K., Darowna, D. & Mozia, S. 2019. Overview of photocatalytic membrane reactors in organic synthesis, energy storage and environmental applications. *Catalysts* 9: 239. https://doi.org/10.3390/catal9030239.

Moridon, S.N.F., Salehmin, M.N.I., Arifin, K., Minggu, L.J. & Kassim, M.B. 2021. Synthesis of cobalt oxide on FTO by hydrothermal method for photoelectrochemical water splitting application. *Applied Sciences* 11: 3031. https://doi.org/10.3390/app11073031.

Moridon, S.N.F., Salehmin, M.I., Mohamed, M.A., Arifin, K., Minggu, L.J. & Kassim, M.B. 2019. Cobalt oxide as photocatalyst for water splitting: Temperature-dependent phase structures. *International Journal Hydrogen Energy* 44: 25495-25504. https://doi.org/10.1016/j.ijhydene.2019.08.075.

Niu, Y., Li, F., Yang, K., Wu, Q., Xu, P. & Wang, R. 2018. Highly efficient photocatalytic hydrogen on CoS/TiO_2 photocatalysts from aqueous methanol solution. *International Journal of Photoenergy* 2018: Article ID. 8143940. https://doi.org/10.1155/2018/8143940.

Ouyang, W., Liu, S., Yao, K., Zhao, L., Cao, L., Jiang, S. & Hou, H. 2018. Ultrafine hollow TiO_2 nanofibers from core-shell composite fibers and their photocatalytic properties. *Composites Communications* 9: 76-80. https://doi.org/10.1016/j.coco.2018.06.006.

Rambey, M.N., Arifin, K., Minggu, L.J. & Kassim, M.B. 2020. Cobalt sulfide as photoelectrode of photoelectrochemical hydrogen generation from water. *Sains Malaysiana* 49(12): 3117-3123. http://dx.doi.org/10.17576/jsm-2020-4912-24.

Rosen, M.A. & Koohi-Fayegh, S. 2016. The prospects for hydrogen as an energy carrier: An overview of hydrogen energy and hydrogen energy systems. *Energy, Ecology and Environment* 1: 10-29. https://doi.org/10.1007/s40974-016-0005-z

Scott, K. 2019. Chapter 1: Introduction to electrolysis, electrolysers and hydrogen production, in electrochemical methods for hydrogen production. *The Royal Society of Chemistry's Books* pp. 1-27. https://doi.org/10.1039/9781788016049-00001

Wang, Q., An, N., Bai, Y., Hang, H., Li, J., Lu, X., Liu, Y., Wang, F., Li, Z. & Lei, Z. 2013. High photocatalytic hydrogen production from methanol aqueous solution using the photocatalysts CuS/TiO_2. *International Journal of Hydrogen Energy* 38(25): 10739-10745. https://doi.org/10.1016/j.ijhydene.2013.02.131

*Corresponding author; email: khuzaim@ukm.edu.my